Battery Thermal Management Systems Design Considering Model Fidelity Levels and Design Optimization Utility

Nowsheen Sharmili*
University of Illinois at Urbana-Champaign, Urbana, IL 61801

Yong Hoon Lee†
The University of Memphis, Memphis, TN 38152

James T. Allison‡
University of Illinois at Urbana-Champaign, Urbana, IL 61801

The electrification of transportation requires a robust and efficient design of battery thermal management systems (BTMSs). This study introduces a resistance-capacitance (RC) based reduced order model (ROM) with additional auxiliary state variables for accurately capturing transient thermal behavior. The study explores the trade-offs between model fidelity and utility in BTMS control co-design (CCD) applications. BTMSs manage the temperature to ensure battery performance, safety, and longevity. Although computational fluid dynamics (CFD) is useful in steady and transient battery thermal analysis, full-fidelity CFD simulations are computationally expensive, particularly within CCD optimization loops. RC-based ROMs commonly used in early-stage design can mitigate the computational effort. These models can be formulated at different fidelity levels by representing various battery components as single or multiple LC bodies connected by resistance elements. The proposed augmented RC-based ROM enhances transient simulation accuracy while maintaining low computational cost, thereby, facilitating thorough design exploration using the CCD approach. This study focuses on comparing model fidelity levels, and their quantifiable utility measures, such as design accuracy and computational cost.

I. Introduction

Thermal runaway is a chain reaction process in which the decomposition of battery materials leads to smoke and explosion. A robust and efficient battery thermal management system (BTMS) is crucial in regulating the temperature within an appropriate range at all times to reduce the likelihood of this phenomenon [1, 2]. BTMS effectiveness is assessed through two primary metrics: the maximum temperature increase and the largest temperature difference within the battery pack [3]. Computational Fluid Dynamics (CFD) has become a common tool for analyzing the transient behavior of battery systems, despite its sometimes significant computational expense and challenges with numerical domain decomposition that can require repeated human inputs [4, 5]. Heat transfer models in CFD are simplified in representing heat exchanges between cells within the battery pack and heat dissipation to the environment with a continuum perspective, and the heat generation is provided directly to the battery zone in terms of a time-dependent volumetric heat source.

In electrochemical battery modeling, physics-based electrochemical models are available to accurately predict the reactive behaviors within individual battery cells [6]. However, for real-time simulation, equivalent circuit models offer simplifications for concurrently predicting the battery electrochemical and thermal behaviors for control-oriented studies [7]. First-order resistance-capacitance (RC) and second-order resistance (dual polarization) models are some of the equivalent circuit models that have been developed.

Reduced order models (ROMs) based on a first-order lumped capacitance (LC) model are typically preferred for their accuracy and simplicity in estimating electric charge, cell voltage, and temperature states [8]. These ROM approaches integrate seamlessly with time-domain simulation via ordinary differential equation (ODE) solvers or direct collocation methods [9].

*Graduate Assistant, Industrial and Enterprise Systems Engineering, 104 S. Mathews Ave. #406, Urbana, IL 61801, AIAA Student Member
†Corresponding author, Assistant Professor, Mechanical Engineering, 312 Engineering Science Building, Memphis, TN 38152, AIAA Member
‡Associate Professor, Industrial and Enterprise Systems Engineering, 104 S. Mathews Ave. #313, Urbana, IL 61801, AIAA Senior Member

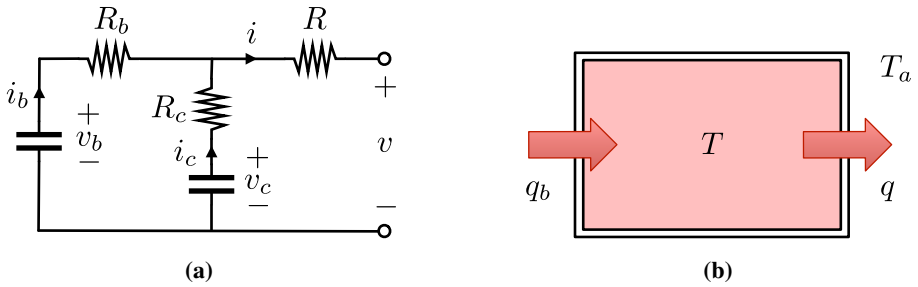

Fig. 1 RC model for a single battery cell. (a) Electric circuit model; (b) Thermal model

Despite the high efficiency of RC-based ROMs in depicting the transient thermal behavior of complex thermal systems, they exhibit several disadvantages. The primary limitation of the simple RC method is its inability to accurately model time-dependent thermal behaviors in some cases. For instance, when a relatively small number of RC bodies are used, the temperature of capacitance bodies instantly reacts to the change of boundary or interface conditions due to a smeared abstraction of the material. Therefore, simple RC methods using a small number of bodies may inaccurately predict delayed temperature responses. While multiple layers of RC bodies can more accurately depict delayed responses, this results in increased model complexity.

The conflict between model accuracy and computational expense is especially important to navigate when constructing models for use with design optimization studies. Accurate models support identification of designs that are better in reality, but with increased computational expense. Such studies are of increasing importance for new emerging technologies without significant design heritage, such as electric vehicles. Integrated design optimization studies can help identify superior designs that may be non-obvious to domain experts, especially for systems using new technology. One class of integrated design optimization studies is Control Co-Design (CCD)[10], which leverages coupling between physical and control system design decisions to reveal high-performance designs. CCD has proven to be an impactful engineering design decision support strategy, including transformative impacts on energy systems [11]. Successful CCD studies requires system models that 1) captures important system transients, 2) accounts for physical system design changes, 3) has reasonable levels of computational expense, and 4) has sufficient accuracy in terms of identifying optimization solutions that translate to high-performance systems in reality.

In this article we introduce a strategy for producing BTMS ROMs that meet the needs of future CCD optimization studies. Specifically, this strategy addresses the issues identified above regarding the shortcomings of RC models through strategic enhancement of these models. We introduce an augmented RC-based ROM with auxiliary state variables that supports prediction of key transient behaviors. Building on the basic RC-based ROM, we integrate auxiliary state variables and their associated model parameters into the state space model. These model parameters are trained using transient simulation results from higher-fidelity CFD models through system identification techniques. This method allows the lower-fidelity state space model to accurately capture delayed transient temperature changes in response to time-varied thermal loadings. Moreover, the augmented RC-based ROM provides more accurate results with lower computational cost compared to the expensive CFD model and simplified LC model.

The rest of the paper is organized as follows. Section II explains the modeling methodologies used in this study. In Sect. II.A, the battery control system for the battery cell is described. In Sect. II.B, the CFD model for the battery thermal management system has been delineated. In Sect. II.C, the solutions for the state space model are presented. Sect. II.D, presents the proposed framework for the additional state model. In Sect. III and Sect. IV, results and conclusions of the paper are described, respectively.

II. Methods

A. Battery Control System for Single Battery Cell

The resistance-capacitance battery model for a single cell (Ref. [12, 13]) is presented in Fig. 1(a). The model consists of two capacitors and three resistors to represent slower and faster electric charge and discharge behaviors of the battery cell. The capacitor C_b reflects the main storage capacitance of the battery, whereas C_c models the fast charge-discharge aspect of the battery, which is substantially smaller than C_b. Here, the RC-based battery cell model is

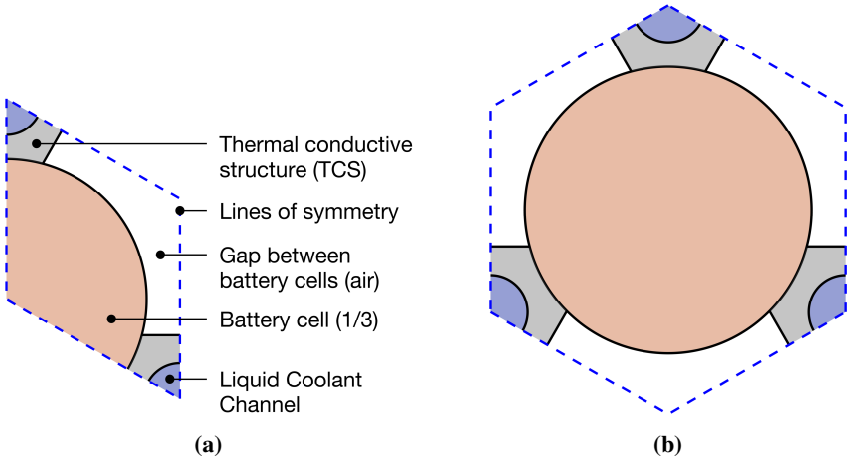

Fig. 2 Cross-section view of three-dimensional battery cell computational model. (a) One third battery cell model; (b) Full battery cell model. Dashed lines denote symmetric boundary condition.

derived in the following series of equations. First, potential drops across the resistors using Ohm's law are represented in Eqns. (1) and (2), given as:

$$C_b \dot{v}_b = -i_b \tag{1}$$

$$C_c \dot{v}_c = -i_c, \tag{2}$$

where, $\dot{v}_b$ is the rate of change of the voltage for the C_b, i_b is the current through the C_b, $\dot{v}_c$ is rate of change of the voltage for the capacitor C_c, and i_c is the current through the capacitor C_c. By applying Kirchhoff's second law in the left loop of the circuit shown in Fig. 1(a) we obtain:

$$v_b - i_b R_b = v_c - i_c R_c, \tag{3}$$

where v_b is the voltage rate for the capacitor C_b, R_b is the resistance for the leftmost junction in Fig. 1(a), v_c is the voltage for the capacitor C_c, and R_c is is the resistance for the rightmost junction in Fig. 1(a). Electrical current conservation in the junction requires that:

$$i = i_b + i_c, \tag{4}$$

where i is the terminal current. Kirchhoff's second law can also be applied to the right loop of the circuit, given as:

$$v = v_c - i_c R_c - iR, \tag{5}$$

where v is the terminal voltage and R is the terminal resistance. Now, heat balances between input and output are represented by Eqns. (6) and (7), given as:

$$q = \frac{T - T_a}{R_T} \tag{6}$$

$$C_T \dot{T} = q_b - q - q_{ac}, \tag{7}$$

where q is the conduction heat transfer rate in watts (W), q_{ac} is the convection heat transfer rate from battery to thermally conductive structures (TCS) air domain in (W), T is the cell temperature, T_a is the ambient or surrounding temperature, R_T is the equivalent thermal resistance in °C/W, C_T is the equivalent heat capacitance in J/°C, $\dot{T}$ is the rate of change of cell temperature, and q_b is the heat generation rate within the cell in W. Note that the heat transfer rate (q_b) generated by the battery cell is conducted through the battery cell (q).

B. CFD Model

In this study, a liquid-cooled BTMS is used for cooling the battery pack. The battery pack is comprised of cylindrical battery cells (specifically, Lithium-ion 18650 battery cells), base plates, integrated circuit (IC) control units, and liquid

channels with heat conduction devices. Each cell in this system is encased by three thermally conductive structures (TCS). Notably, each TCS incorporates a cylindrical liquid channel at its center for liquid coolant flow. The design of each TCS features three curved thermal contacts, the curvature radius of which matches the radius of the cylindrical battery cell [14]. The cooling water is distributed from an upper reservoir and flows into each TCS in parallel. The heat generated by the batteries is conducted to the TCS and dissipated via convection by the cooling water. The heated coolant exits the system through an outlet in the bottom reservoir. This study employs a one-third battery cell model, with symmetry assumptions illustrated in Fig. 2(a). Another option for the same configuration is a full battery cell model, shown in Fig. 2(b). However, due to physical symmetry, the one-third model is sufficient to capture important thermal behaviors.

The Li-ion battery is assumed to be composed of NCR material (i.e., Lithium nickel cobalt aluminum oxide, or LiNiCoAlO2). Aluminum is used for the TCS material, and water is used for liquid coolant. The numerical studies have been conducted using a pressure-based segregated CFD solver formulation with the energy transport equation and SST k-ω turbulence model. Initially, steady state analysis has been performed in the one-third battery cell model using a mass flow rate inlet of 10^{-5} kg/s. The maximum heat generation rate of the battery for the maximum power output has been quantified in 12. Considering the convergence rate, at least 2,000 iterations (with an algebraic multigrid technique) were performed for all simulation cases. The temperature and pressure of the TCS flow channel entry and exit are reported based on stable steady state analysis. Moreover, the heat transfer rate from battery cell to TCS air domain (q_{ac}) and the surrounding temperature of the TCS air domain (T_a) are calculated from a similar stable steady-state model. These parameters are provided to the LC model to construct the state space equations.

1. Heat Capacitance Calculation

The specific heat capacity of the battery is determined through the specific heat capacity of its constituent materials [15]. The specific heat capacity of the cell can be expressed via the subsequent equation, given as:

$$c_p = \frac{\sum_i \rho_i c_i V_i}{\rho \sum_i V_i}, \tag{8}$$

where ρ and ρ_i denote the density of the cell and the cell constituent materials, respectively. The specific heat capacity of the cell and the constituent materials are denoted as c_p and c_i, respectively. The volume of the cell constituent is represented by V_i. The heat capacitance is calculated by dividing the specific heat by the cell mass [16].

2. Equivalent Resistance Calculation

Equivalent thermal resistance is characterized as the ratio of the temperature difference across two surfaces of a material to the rate of heat flux per unit area [17]. Greater thermal resistance indicates less heat loss. Thermal resistance value depends on both the thermal conductivity and the thickness between two surfaces of the material. The thermal resistance (R_T) can be expressed by the subsequent equation, given as:

$$R_T = \frac{h}{\lambda}, \tag{9}$$

where h is the thickness towards the flow channel and λ is the thermal conductivity of the material.

C. State Space Solution

The state space equations can be solved using general ODE solvers, such as `ode45` in MATLAB. To model the delayed thermal relaxation from the LC bodies, two auxiliary states, ψ_1 and ψ_2, have been integrated in the state space model. These auxiliary states aim to modulate the time-dependent response of the original state variable that denotes the component temperature, thus mimicking the delayed temperature responses of the real thermal system. Their coefficients have dependencies with each other and on temperature. The augmented state space equations are derived below.

The state space equations for voltage rates $\dot{v}_b$ and $\dot{v}_c$ are given as:

$$\begin{aligned} \dot{v}_b &= \frac{(v_b - v_c)}{(R_c + R_b)C_b} + \frac{R_c i}{(R_c + R_b)C_b}, \\ \dot{v}_c &= \frac{(v_c - v_b)}{(R_c + R_b)C_c} + \frac{R_b i}{(R_c + R_b)C_c}. \end{aligned} \tag{10}$$

These two voltage rates both depend on quantities: v_b, v_c, R_c, R_b, C_c, and i. The state space equation for the rate of cell temperature change is given as:

$$\dot{T} = \frac{q_b}{C_T} - \frac{T}{C_T R_T} + \frac{T_a}{C_T R_T} - \frac{q_{ac}}{C_T}, \tag{11}$$

which is derived by substituting Eqn. (6) into Eqn. (7).

According to Ref. [18], the internal heat generation rate of a Li-ion battery (LIB) can be divided into the following parts: polarization reaction heat, joule heat, chemical reaction heat, and electrolyte and solid electrolyte interphase (SEI) layer decomposition. Among the theoretical algorithms to estimate the heat production rate of batteries, a well-established option is the one proposed in Ref. [19] where the heat generation rate of battery can be given as:

$$q_b = i^2 R - iT' \left(\frac{dU_{oc}}{dT} \right) \tag{12}$$

In this equation, q_b is the heat generation rate of the battery cell, i is the discharge current of the battery cell and dU_{oc}/dT is the temperature coefficient of open-circuit voltage. An equivalent resistance R is obtained during the discharge process. The equivalent resistance R and the temperature coefficient (dU_{oc}/dT) are quantified in [20] by means of an empirical relation between state of charge (SOC), dU_{oc}/dT, and the equivalent resistance R for a particular cell temperature T'. By using Eqns. (1) through (7), (11), and (12), the equation of the cell temperature change rate can be formulated as:

$$\dot{T} = \frac{i^2 R - iT' \left(\frac{dU_{oc}}{dT} \right)}{C_T} - \frac{T}{C_T R_T} + \frac{T_a}{C_T R_T} - \frac{q_{ac}}{C_T}, \tag{13}$$

The state space equation for the rate of cell temperature change with the two additional auxiliary states, ψ_1 and ψ_2, is then represented by:

$$\begin{aligned} \dot{T} = & \frac{i^2 R - iT' \left(\frac{dU_{oc}}{dT} \right)}{C_T} - \frac{T}{C_T R_T} + \frac{T_a}{C_T R_T} - \frac{q_{ac}}{C_T} \\ & + \mathcal{F}\left[\psi_1, \psi_2\right], \end{aligned} \tag{14}$$

where $\mathcal{F}$ is an arbitrary function consisting of ψ_1 and ψ_2. The state space equation of the rate of change of these auxiliary variables is given as:

$$\begin{aligned} \dot{\psi}_1 &= \dot{\psi}_1\left(\psi_1, \psi_2\right), \\ \dot{\psi}_2 &= \dot{\psi}_2\left(\psi_1, \psi_2\right). \end{aligned} \tag{15}$$

Here, without considering the additional auxiliary state variables, the overall state space equations are given as:

$$\frac{d}{dt} \begin{bmatrix} v_b \\ v_c \\ T \end{bmatrix} = \begin{bmatrix} \frac{(v_b - v_c)}{(R_c + R_b)C_b} + \frac{R_c i}{(R_c + R_b)C_b} \\ \frac{(v_c - v_b)}{(R_c + R_b)C_c} + \frac{R_b i}{(R_c + R_b)C_c} \\ \frac{i^2 R - iT' \left(\frac{dU_{oc}}{dT} \right)}{C_T} - \frac{T}{C_T R_T} + \frac{T_a}{C_T R_T} - \frac{q_{ac}}{C_T} \end{bmatrix}. \tag{16}$$

Due to the nonlinearity of the rate of the temperature change equation, the overall state space equation cannot be represented in a linear form. With the additional auxiliary variables, the equation now includes an additional term in the rate of temperature change equation. Here, we assume all arbitrary relationships involving the auxiliary state variables are linear. The rate of temperature change is assumed to linearly depend upon all auxiliary state variables (ψ_1 and ψ_2).

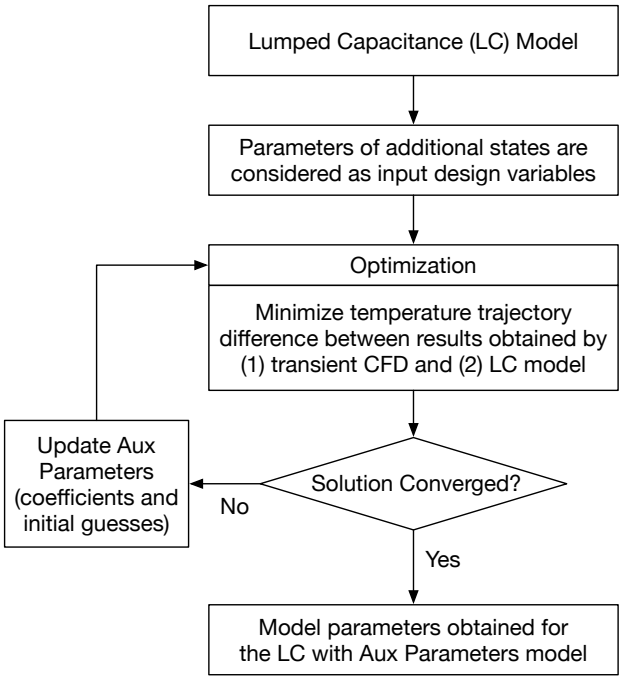

Fig. 3 Proposed Framework for Additional State Model

With these assumptions, the state space equations with the additional auxiliary state variables can be represented as:

$$\frac{d}{dt}\begin{bmatrix} v_b \\ v_c \\ T \\ \psi_1 \\ \psi_2 \end{bmatrix} = \begin{bmatrix} \dfrac{(v_b - v_c)}{(R_c + R_b)C_b} + \dfrac{R_c i}{(R_c + R_b)C_b} \\ \dfrac{(v_c - v_b)}{(R_c + R_b)C_c} + \dfrac{R_b i}{(R_c + R_b)C_c} \\ \dfrac{i^2 R - iT'\left(\dfrac{dU_{oc}}{dT}\right)}{C_T} - \dfrac{T}{C_T R_T} + \dfrac{T_a}{C_T R_T} - \dfrac{q_{ac}}{C_T} \\ \quad + a_{34}\psi_1 + a_{35}\psi_2 \\ a_{44}\psi_1 + a_{45}\psi_2 \\ a_{54}\psi_1 + a_{55}\psi_2 \end{bmatrix}. \tag{17}$$

where the state variables for this set of state space equations are v_b, v_c, T, ψ_1, and ψ_2. The unknown coefficients of the state space equation are identified here via least square minimization of two transient temperature response curves from the transient CFD model and the augmented RC-based ROM formulated in Eqn. (17). To facilitate the easier numerical discovery of these unknown coefficients, an additional constraint is included in the optimization problem that requires the peak temperatures must be equal. With this augmented RC-based ROM approach, a single one-third battery cell model will be trained.

D. Proposed Framework with Additional States

The additional state model is a simplified model which predicts the system behavior similar to the transient analysis with a low computational cost. The proposed framework for the additional state model is depicted in Fig 3. The parameters of the additional state are considered as optimization variables, and they are obtained by minimizing

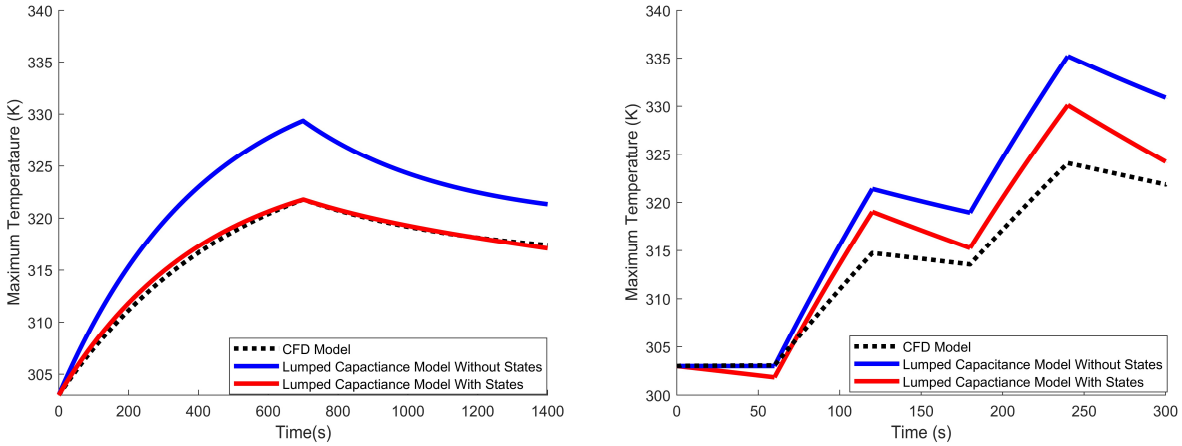

(a) Constant heat load scenario **(b) Continuous on-off Scenario**

Fig. 4 Battery load scenarios

temperature trajectory differences between results obtained by transient CFD and LC models, given as:

$$\begin{aligned} &\text{minimize} \quad \left(\sum_{n=0}^{n} T_{\text{lumped}}(i) - \sum_{n=0}^{n} T_{\text{transient}}(i)\right)^2 + \rho \left(TA_{\text{lumped}} - TA_{\text{transient}}\right)^2 \\ &\text{subject to} \quad T_{L,\max} = T_{T,\max} \end{aligned} \tag{18}$$

The objective function for minimization is the difference between the temperature trajectory points predicted by the LC model and the transient analysis. The temperature trajectory area between the LC and the transient analysis is penalized in the objective function with penalty parameter, ρ. The peak temperature of the transient analysis $T_{T,\max}$ and the LC model $T_{L,\max}$ is constrained explicitly in the optimization problem as an equality constraint.

III. Results

The simulation of electric vehicles for various operating conditions is crucial to avoid the thermal runaway, which can lead to fire and explosions. In this study, the electric vehicle simulation is conducted for different scenarios such as constant heat load and continuous on-off conditions with models under various fidelity levels, and compared for the potential use in CCD optimization problems. In the constant heat load case, the battery is discharged with an interval of 700 s with two heat loads. Another scenario is to continuously turn on and off the battery with a particular depth of discharge. The transient analysis has been conducted using the CFD model (defined in Sect. II.B) with varying time whereas the LC model without and with additional states have been formulated using state space representation (defined in Sect. II.C).

The LC model predicts the trend of the transient system behavior in simplified way, giving rough predictions of the system behaviors. The proposed LC model with additional states is formulated to approximately forecast the transient simulation more closely by compensating the errors using additional states, with associated parameters trained by data-driven approach. The comparison plot between LC model and transient analysis for constant heat load and continuous on-off scenario are illustrated in Fig. 4a and Fig. 4b. The LC model with additional states illustrates a trend similar to the transient simulation with less computational error than the LC model without states. Moreover, the LC model with additional states performs well even in complicated situations, i.e., continuous on-off scenarios. However, the computational error of the LC model with additional states for the continuous on-off scenario is larger than the constant heat load case due to multiple reasons.

First, the training did not enforce thermodynamic conservation laws. The additional state model parameters are trained from a purely data-driven point of view. The curves from the LC model with additional states closely track the responses of the CFD model results with good accuracy. However, the absence of thermodynamic conservation enforcement might cause failure in highly complex scenarios outside of system designers' prediction range, such as

Table 1 Computational Cost for Different Model Fidelity Levels

Model Fidelity Case	Computational Times (s)			
	Add. state training		Constant heat load	Continuous on-off
	Ref CFD	Training		
CFD Model	N/A	N/A	12,420	2,700
LC Model	N/A	N/A	0.5417	1.162
LC Model with Additional States	5,400	1,160	3.081	2.614

continuous change of utilization modes. In this study, this type of complexity is represented using the continuous on-off scenario. Specifically, in this scenario, energy conservation is not maintained during the initial 60 s. The cooling slope is significantly steeper than the CFD model in a time range from 240 to 300 s. These two observations are strong clues that energy conservation needs to be enforced in an improved reduced order model with additional states.

Second, related to the non-conservative nature, adjusting the additional parameters in the model during training may artificially reduce the temperature change slopes, because the model parameters are trained using an initial guess from the over-predicting model (simple LC-model) and the data-driven training tries to make these temperature trajectories closer to the higher-fidelity CFD responses. This reduces the overall derivative response, causing over-cooling behavior in the prediction. To avoid this situation, there is a need for training the additional state parameters in heating and cooling phases separately.

The optimization problem implemented in the current framework relies on matching the points and area between the CFD and the LC model. Considering the energy flux and using gradient-enhanced Kriging (GEK, Ref. [21]) may mitigate these limitations, especially when considering energy flux as an added constraint. Additionally, the current LC model with additional states consists of two linearly-posed states, which is a minimal implementation for technical demonstration. Increasing the number of states and allowing nonlinear auxiliary states may facilitate capturing more accurate system behavior with greater accuracy.

The comparison between the computational costs for transient CFD model, LC model, and LC model with states is depicted in Tab. 1. Based on the computational time in this comparison, the CFD model requires orders of magnitude higher computational time for solving the transient conjugate heat transfer problems, which are quantified as 12,420 s and 2,700 s for each of two scenarios (constant heat load and continuous on-off). This high computational demand renders it unsuitable for efficient optimization of control strategies. However, these simulation cases are still useful when accurately tuning the lower-fidelity models, such as LC model with additional states. For model training purposes, the master CFD simulation case consists of both constant heat load and continuous on-off discharge scenarios, and computation required approximately 5,400 s for running the master CFD simulation case, and model training optimization process required an additional 1,160 s, resulting in a total model training cost of 6,560 s. The training time for the additional states is not small, but model training needs to be performed only once, so large training time is not a concern in cases where multiple optimization studies will be performed (a common situtation).

The LC model with additional states has orders of magnitude lower computational time compared to the transient CFD model. The computational times for the LC model with additional states are quantified as 3.081 s for constant heat load and 2.614 s for continuous on-off scenarios. Still, compared with the pure LC model cases, quantified as 0.5417 s for constant heat load and 1.162 s for continuous on-off scenarios, the LC model with additional states cases have higher computational time. However, these differences are not a significant concern given the comparatively significant CFD computational times.

For better visualization, the error analysis is shown in Fig. 5, where the CFD temperature (black dashed line) is regarded as the reference temperature. Figure5a illustrates that the error is lower for the additional states model than for the LC model for constant heat load scenario. In addition, from Fig. 5b, by analyzing the slopes, it can be seen that the error quantity is lower for the additional states model than the LC model for continuous on-off scenario. The LC model with additional states is therefore computationally efficient both in terms of accuracy and computational time.

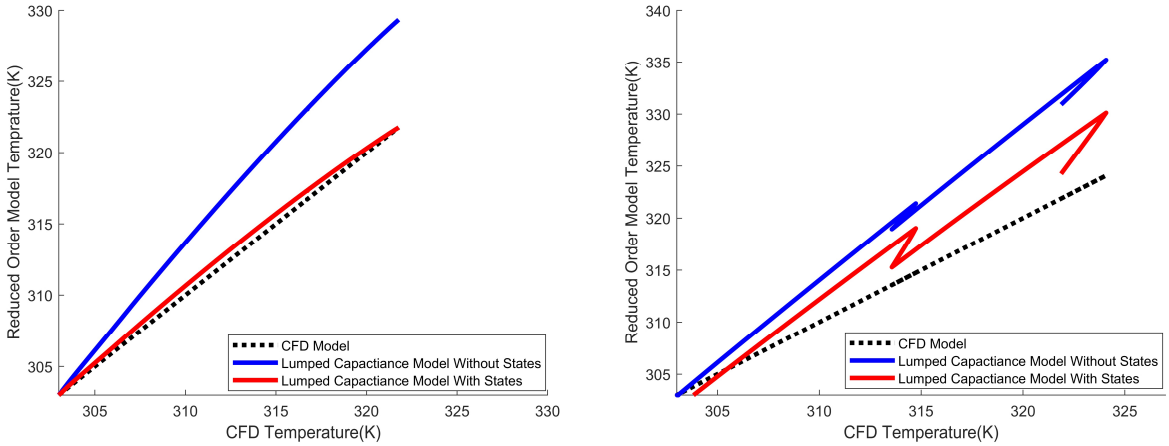

(a) Constant heat load scenario **(b) Continuous on-off Scenario**

Fig. 5 Reduced order model error analysis

IV. Conclusion

In this study, we compared model responses, encompassing the one-third battery cell CFD model, traditional RC-based ROM, and our proposed augmented RC-based ROM. The augmented RC-based ROM approach offers a novel way to accurately predict delayed temperature response in transient thermal analysis, without substantially increasing costs. The augmented RC-based ROM model shows similar trend as the transient CFD model with lower computational cost for both constant heat load and continuous on-off discharge scenarios. Moreover, among different model fidelity levels, the LC model with additional states simultaneously addresses the computational cost issue of the expensive CFD model and the error issue of the simplified LC model. The current LC model with additional states framework has a limitation in capturing the exact system behavior in continuous on-off scenarios due to its noisy function nature. The incorporation of the GEK and increasing the number of auxilliary states may ameliorate this limitation. Future work is planned to complete additional comparative studies with alternative additional state ROMs (expanding our knowledge of this strategy, and to solve CCD optimization problems using these models, comparing design utility metrics and demonstrating the relationship between design solution accuracy and computational optimization efforts, including human modeling effort and computational cost. The expected outcomes of this research will offer valuable insights into developing thermal models for battery systems, contributing not only to simulating existing systems but also to facilitating design exploration and optimization using CCD approaches.

Acknowledgment

The authors would like to give special thanks to Dr. Ruben Andres Salas Varela for his role to develop the objective function formulation for the proposed additional state framework. He also assisted to understand the nature of the state space model.

References

[1] Liu, T., Liu, Y., Wang, X., Kong, X., and Li, G., "Cooling control of thermally-induced thermal runaway in 18,650 lithium-ion battery with water mist," *Energy Conversion and Management*, Vol. 199, 2019, p. 111969. https://doi.org/10.1016/j.enconman.2019.111969.

[2] Liu, T., Tao, C., and Wang, X., "Cooling control effect of water mist on thermal runaway propagation in lithium-ion battery modules," *Applied Energy*, Vol. 267, 2020, p. 115087. https://doi.org/10.1016/j.apenergy.2020.115087.

[3] Lin, J., Liu, X., Li, S., Zhang, C., and Yang, S., "A review on recent progress, challenges and perspective of battery thermal management system," *International Journal of Heat and Mass Transfer*, Vol. 167, 2021, p. 120834. https://doi.org/10.1016/j.ijheatmasstransfer.2020.120834.

[4] Inui, Y., Kobayashi, Y., Watanabe, Y., Watase, Y., and Kitamura, Y., "Simulation of temperature distribution in cylindrical and prismatic lithium-ion secondary batteries," *Energy Conversion and Management*, Vol. 48, No. 7, 2007, pp. 2103–2109. https://doi.org/10.1016/j.enconman.2006.12.012.

[5] Vu, H., and Shin, D., "Scheduled pre-heating of Li-ion battery packs for balanced temperature and state-of-charge distribution," *Energies*, Vol. 13, No. 9, 2020, p. 2212. https://doi.org/10.3390/en13092212.

[6] He, W., Pecht, M., Flynn, D., and Dinmohammadi, F., "A physics-based electrochemical model for lithium-ion battery state-of-charge estimation solved by an optimised projection-based method and moving-window filtering," *Energies*, Vol. 11, No. 8, 2018, p. 2120. https://doi.org/10.3390/en11082120.

[7] Zhang, L., Peng, H., Ning, Z., Mu, Z., and Sun, C., "Comparative research on RC equivalent circuit models for lithium-ion batteries of electric vehicles," *Applied Sciences*, Vol. 7, No. 10, 2017, p. 1002. https://doi.org/10.3390/app7101002.

[8] Rajchapanupat, N., and Poramapojana, P., "A comparative study of equivalent circuit models for a Li-ion battery pack of an electric Tuk-Tuk," *IOP Conference Series: Materials Science and Engineering*, Vol. 1137, No. 1, 2021, p. 012014. https://doi.org/10.1088/1757-899X/1137/1/012014.

[9] Rao, A. V., "A survey of numerical methods for optimal control," *Advances in the Astronautical Sciences*, Vol. 135, No. 1, 2010, pp. 497–528.

[10] Allison, J. T., and Herber, D. R., "Multidisciplinary Design Optimization of Dynamic Engineering Systems," *AIAA journal*, Vol. 52, No. 4, 2014, pp. 691–710.

[11] Garcia-Sanz, M., "Control Co-Design: an Engineering Game Changer," *Advanced Control for Applications: Engineering and Industrial Systems*, Vol. 1, No. 1, 2019, p. e18.

[12] Markel, T., Brooker, A., Hendricks, T., Johnson, V., Kelly, K., Kramer, B., O'Keefe, M., Sprik, S., and Wipke, K., "ADVISOR: a systems analysis tool for advanced vehicle modeling," *Journal of Power Sources*, Vol. 110, No. 2, 2002, pp. 255–266. https://doi.org/10.1016/S0378-7753(02)00189-1.

[13] Johnson, V. H., "Battery performance models in ADVISOR," *Journal of Power Sources*, Vol. 110, No. 2, 2002, pp. 321–329. https://doi.org/10.1016/S0378-7753(02)00194-5.

[14] Lai, Y., Wu, W., Chen, K., Wang, S., and Xin, C., "A compact and lightweight liquid-cooled thermal management solution for cylindrical lithium-ion power battery pack," *International Journal of Heat and Mass Transfer*, Vol. 144, 2019, p. 118581. https://doi.org/10.1016/j.ijheatmasstransfer.2019.118581.

[15] Tang, Y., Li, T., and Cheng, X., "Review of specific heat capacity determination of lithium-ion battery," *Energy Procedia*, Vol. 158, 2019, pp. 4967–4973. https://doi.org/10.1016/j.egypro.2019.01.671.

[16] Lobontiu, N., *System Dynamics for Engineering Students: Concepts and Applications*, Academic Press, London, UK, 2017.

[17] Mishra, R., Militky, J., and Venkataraman, M., "Nanoporous Materials," *Nanotechnology in Textiles: Theory and Application*, Woodhead Publishing, Sawston, UK, 2019, Chap. 7, pp. 311–353. https://doi.org/10.1016/B978-0-08-102609-0.00007-9.

[18] Li, D., Wang, L., Duan, C., Li, Q., and Wang, K., "Temperature prediction of lithium-ion batteries based on electrochemical impedance spectrum: A review," *International Journal of Energy Research*, Vol. 46, No. 8, 2022, pp. 10372–10388. https://doi.org/10.1002/er.7905.

[19] Bernardi, D., Pawlikowski, E., and Newman, J., "A general energy balance for battery systems," *Journal of The Electrochemical Society*, Vol. 132, No. 1, 1985, pp. 5–12. https://doi.org/10.1149/1.2113792.

[20] Lai, Y., Wu, W., Chen, K., Wang, S., and Xin, C., "A compact and lightweight liquid-cooled thermal management solution for cylindrical lithium-ion power battery pack," *International Journal of Heat and Mass Transfer*, Vol. 144, 2019, p. 118581.

[21] Bouhlel, M. A., and Martins, J. R. R. A., "Gradient-enhanced kriging for high-dimensional problems," *Engineering with Computers*, Vol. 35, No. 1, 2019, p. 157–173. https://doi.org/10.1007/s00366-018-0590-x.